Pure Appl. Geophys. 169 (2012), 1963–1975

DOI 10.1007/s00024-012-0466-8

Pure and Applied Geophysics

$m_b(Pn)$ Scale for the Korean Peninsula and Site-Dependent Pn Amplification

Tae-Kyung Hong[1] and Kiwook Lee[1]

Abstract—The Korean Peninsula is located in the far-eastern Eurasian plate margin where crustal structures vary laterally, causing significant raypath-dependent modulations of crustal phases. The discriminative variations of crustal phases hinder application of conventional local magnitude scales in the continental margin. The mantle-lid phase is less affected by the crustal structures than the crustal phases, providing a better constraint to magnitude estimation. A regional body-wave magnitude scale based on the mantle-lid P wave (Pn), $m_b(Pn)$, is developed for regional events around the Korean Peninsula. The $m_b(Pn)$ scale is determined to be $m_b(Pn) = 0.380\ (\pm 0.299) + \log A + 2.012\ (\pm 0.122) \log d$, where A is the peak-to-peak Pn amplitude in μm and d is the epicentral distance in km. The $m_b(Pn)$ estimates of regional events around the Korean Peninsula are determined. The $m_b(Pn)$ estimates are compared with other available magnitude estimates ($m_b(Lg)$, M_L). The influence of structures beneath stations on Pn amplification is investigated from inter-station magnitude residuals. A characteristic spatial variation of inter-station magnitude residuals with strengths mostly between −6 and 6 %, but with maximum strengths of ±10 %, is observed. The inter-station magnitude residuals appears to be correlated well with geological and seismic structures in the crust.

1. Introduction

The estimation of earthquake size is a fundamental task in seismic monitoring. Small and moderate-size earthquakes are observed only in local and regional distances. Thus, development of magnitude scales based on regional seismic waves is crucial for monitoring of such small and moderate-size earthquakes. Local and regional seismic waves typically travel through the crust and mantle lid. Thus, they are influenced by the lithospheric structures (e.g., Kennett and Furumura, 2001; Hong *et al*., 2008; Hong and Rhie, 2009).

In particular, lateral variation of crustal thicknesses causes high variability in the amplitudes of regional crustal phases, raising phase-dependent discriminative attenuation (Kennett, 1986; Hong *et al*., 2008).

Local magnitude scales are officially implemented for assessment of event sizes around the Korean Peninsula (KIGAM, 1995; KMA, 1999). It is known that the local magnitude scales are applicable up to near-regional distances in which the path effects can be regarded to be uniform and azimuth-independent (e.g., Kim, 1998). However, lateral crustal structures vary significantly in continental margins, hindering application of local magnitude scales even to near-regional events.

Crustally-guided shear waves (Lg) and mantle-lid P waves (Pn) are often used for regional body-wave magnitude scales. The Lg wave is typically the strongest regional phase in the continental crusts. The Lg body-wave magnitude scales are widely used for measurement of magnitudes in regional continental environments (Nuttli, 1986; Priestley and Patton, 1997; Patton and Schlittenhardt, 2005). However, the Lg waves attenuate strongly in laterally-varying crusts. Thus, proper correction of amplitudes is required for estimation of accurate magnitudes.

The mantle-lid P waves (Pn) develop from P refraction on the Moho. The Pn waves are the first-arrival phase in regional distances, and are well observed in regional seismograms. Thus, the Pn waves are less influenced by the crustal structures than the crustal phases such as Lg. The Pn waves are useful for assessment of event sizes in regions with complex crustal structures such as continental margins. Also, it is known that $m_b(Pn)$ scale is useful for inference of the yields of underground nuclear explosions because compressional energy is excited

[1] Department of Earth System Sciences, Yonsei University, Shinchon-dong, 134, Seodaemun-gu, Seoul 120-749, South Korea. E-mail: tkhong@yonsei.ac.kr

dominantly from the explosions (Vergino and Mensing, 1990; Leach *et al*., 1993).

The Korean Peninsula and its vicinity compose the far-eastern margin of the Eurasian plate in which lateral crustal structures vary abruptly (Cho *et al*., 2004; Chang and Baag, 2005; Kang and Shin, 2006; Hong and Kang, 2009). We develop a *Pn* body-wave magnitude scale for the Korean Peninsula. We compare the $m_b(Pn)$ estimates with other available magnitude estimates. We also calculate the spatial variation of magnitude residuals of $m_b(Pn)$. We investigate the influence of crustal structures beneath stations on *Pn* amplification from spatial variation of magnitude residuals.

2. Geology

The Korean Peninsula belongs to the far-eastern margin of the Eurasian plate, and has experienced complex tectonic history including continental collisions and a rifting (Chough *et al*., 2000; Kim *et al*., 2003). The Korean Peninsula presents typical features of a continental crust where a characteristic Conrad discontinuity is observed (He and Hong, 2010). The lithospheric structure of the Korean Peninsula is composed of three Precambrian massif blocks (Nangnim, Gyeonggi, Yeongnam) and two intervening fold belts (Imjingang, Okcheon) (Fig. 1a). The unification of the massif blocks was completed in the Jurassic (Chough *et al*., 2000).

A Cretaceous volcanic sedimentary basin (Gyeongsang) is located in the southeastern Korean Peninsula (Yin and Nie, 1993; Chough *et al*., 2000). The East Sea (Sea of Japan) was opened during the Oligocene to mid-Miocene, causing development of a passive margin in the region off the east coast of the peninsula. A signature of magmatic underplating is observed in the lower crust of the region (Chough *et al*., 2000; Cho *et al*., 2004). The lateral variation of mantle-lid structures in the Korean Peninsula is close to the observed crustal features, suggesting that the tectonic structures are consistently observed in the lithosphere (Hong and Kang, 2009).

The pure continental crust in the Korean Peninsula changes to a transitional structure between continental and oceanic crusts (Hong and Kang, 2009). The crustal thicknesses are 26–33 km in the Korean Peninsula and Yellow Sea, while they decrease to ~ 12 km in the East Sea (Chang and Baag, 2005; Hong *et al*., 2008). The changes of crustal structures across the east coast of the Korean Peninsula cause significant variations in regional phases (Hong *et al*., 2008; Hong, 2010).

The Korean Peninsula is an intraplate region, incorporating typical crustal earthquakes. These earthquakes occur as a result of effects of compressional stresses induced from plate boundaries around the Japanese subduction zones and India-plate collision margins. Strike-slip earthquakes with fault planes striking in NE-SW or in the conjugate directions are most dominant (Choi *et al*., 2012). Some thrust earthquake occur in the region off the east coast of the Korean Peninsula where the continental rifting responsible for the East Sea opening was initiated. We also find some normal-faulting events at a narrow region in the central Yellow Sea.

3. Data

The number of seismic stations has been increasing in the Korean Peninsula since 1978. The current shape of dense nation-wide seismic networks was formed in 2000. Two major seismic monitoring institutes are the Korea Meteorological Administration (KMA) and the Korea Institute of Geoscience and Mineral Resources (KIGAM). The level of seismicity around the Korean Peninsula is moderate. Small and moderate-size earthquakes are typically observed around the Korean Peninsula. Five earthquakes with magnitudes equal to or greater than $M_L 5.0$ occurred since 1978.

For stable determination of magnitude scale, it is required to analyze waveforms with high signal-to-noise ratios. Considering the ambient noise levels, spatial distribution of events and stations and epicentral distances, regional waveforms from events with magnitudes equal to or greater than $M_L 3.0$ are analyzed (Fig. 1). We collect 7,552 seismic waveforms for 86 regional events during 2000–2010 around the Korean Peninsula. Seismic waveforms and event information are collected from KMA and KIGAM.

In this study, we analyze mantle-lid *P* waves (*Pn*) and their coda wavetrains. The *Pn* is the first-arrival

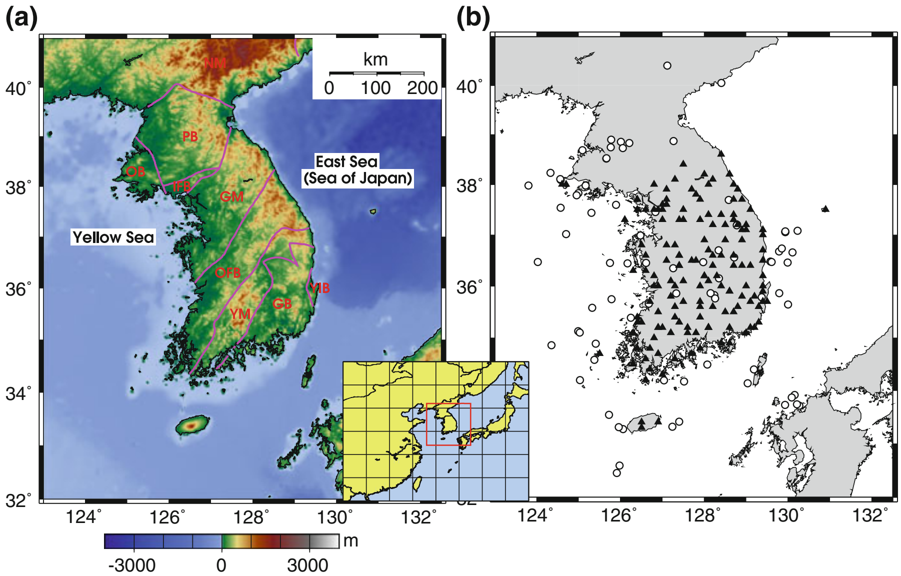

Figure 1

a Map of geological structures in the Korean Peninsula: Gyeongsang basin (GB), Gyeonggi massif (GM), Imjingang fold belt (IFB), Nangrim massif (NM), Ongjin basin (OB), Okcheon fold belt (OFB), Pyeongnam basin (PB), Yeonil basin (YIB), and Yeongnam massif (YM). **b** Map of events and stations. Seismic waveforms for 80 events (*open circles*) recorded at 151 stations (*closed triangles*) are analyzed

phase in regional distances greater than ~130 km in continental lithospheres (e.g., Helmberger *et al.*, 1993). We remove the seismograms with low signal-to-noise ratios, anomalous amplitudes, or epicentral distances less than 150 km. We finally analyze 3,470 vertical seismograms for 80 regional earthquakes around the Korean Peninsula (Fig. 1b; Table 1).

The events are crustal events with focal depths less than 33 km (Table 1). The epicentral distances are 150–700 km. The seismic records were collected from 151 stations in the Korean Peninsula. The seismograms were recorded at short-period and broadband velocity seismometers and accelerometers. We examine every seismogram manually, excluding the waveform records with low *Pn* signal-to-noise ratios. We collect the *Lg* body-wave magnitude estimates ($m_b(Lg)$) for the events from Hong (2012).

4. Methods

4.1. $m_b(Pn)$ Magnitude Scale

We collect *Pn* amplitudes from simulated vertical waveforms on short-period seismometer of the World-Wide Standardized Seismograph Network (SP WWSSN) (Priestley and Patton, 1997). The SP WWSSN waveform records can be simulated by convolving the observed ground motions with the SP WWSSN instrument response. The $m_b(Pn)$ scale based on the vertical SP WWSSN records takes a form (Denny *et al.*, 1987; Priestley and Patton, 1997):

$$m_b(Pn) = a + \log A + b \log d, \qquad (1)$$

where A is the peak-to-peak *Pn* amplitude in μm on SP WWSSN (Fig. 2), d is the epicentral distance in km, and a and b are calibration constants to be determined.

The *Pn* phase is observed as a single wavelet that is typically the first arrival phase in regional distances. In this study, we measure the peak-to-peak *Pn* amplitudes from the vertical record sections following the conventional definition of $m_b(Pn)$ scale, which allows us to retain the transportability of the magnitude scale (e.g., Priestley and Patton, 1997). The peak-to-peak amplitudes A in (1) are measured from the *Pn* and *Pn*-coda wavetrains in time windows bounded by *Pn* and *Pg* traveltime curves (Priestley and Patton, 1997).

The time window range is defined to include the *Pn* and *Pn* coda securely. Considering the *Pn* and *Pg*

Table 1

Source parameters of events analyzed in this study

Date (yyyy/mm/dd)	Time (hh:mm:ss)	Lat (°N)	Ion (°E)	Dep (km)	M_L (KIGAM)	M_L (KMA)	m_b (ISC)	$m_b(Lg)$	$m_b(Pn)$
2000/08/05	12:03:00.0	34.6	125.4	5.3	3.4	2.7	–	3.10	3.47
2000/12/09	09:51:00.0	36.5	130.0	–	3.9	3.7	3.8	4.45	4.11
2001/01/29	02:44:08.6	35.7	126.7	0.8	3.5	3.0	–	3.64	3.67
2001/07/23	08:29:14.6	36.5	128.0	13.6	3.6	3.5	–	3.46	3.31
2001/08/24	02:12:03.5	35.9	128.2	1.7	3.2	3.1	–	3.16	3.21
2001/11/21	01:49:11.6	36.7	128.3	0.5	3.6	3.5	–	3.84	3.69
2001/11/24	07:10:32.0	36.7	129.9	7.1	4.1	4.1	4.1	4.23	3.84
2002/03/07	14:30:57.2	36.4	126.6	0.3	3.2	3.0	–	3.04	3.68
2002/03/17	00:26:41.1	38.2	124.5	33.0	3.8	3.9	4.2	4.13	4.27
2002/03/22	02:28:55.2	38.1	124.6	1.3	3.0	3.5	–	3.13	3.67
2002/04/16	22:52:38.6	40.7	128.7	10.0	3.4	3.9	4.1	4.87	4.39
2002/07/08	19:01:49.9	35.9	129.8	11.5	3.7	3.8	–	4.13	3.80
2002/07/16	21:50:30.7	38.0	125.2	0.8	3.4	3.3	–	3.38	3.71
2002/09/17	09:08:11.8	36.5	124.0	2.3	3.6	–	–	3.86	4.08
2002/12/09	22:42:49.8	38.9	127.3	0.7	4.1	3.8	–	4.15	3.96
2003/01/09	08:33:21.2	37.5	124.6	5.0	3.9	3.9	3.3	4.14	4.02
2003/03/01	14:33:28.5	35.8	129.4	10.4	3.2	3.0	–	3.31	3.51
2003/03/09	18:28:03.2	36.1	128.4	1.2	3.1	3.1	–	3.22	3.55
2003/03/22	20:38:40.4	35.0	124.4	10.0	5.1	4.9	4.7	5.41	5.11
2003/03/30	11:10:57.0	38.0	123.8	4.5	4.8	5.0	–	5.65	5.21
2003/04/15	17:55:23.9	36.4	126.2	0.7	3.5	3.3	–	3.55	3.44
2003/07/05	03:18:29.9	37.4	125.3	5.0	3.1	3.0	–	3.19	3.75
2003/10/13	09:12:04.9	37.0	126.5	5.4	3.9	3.6	–	4.12	4.04
2004/01/05	16:49:42.9	38.7	125.1	1.0	3.4	3.2	–	3.53	3.50
2004/04/26	04:29:25.0	35.8	128.2	8.2	4.0	3.9	–	4.11	4.22
2004/05/05	03:22:27.8	32.4	125.9	0.0	3.0	3.1	–	3.50	3.79
2004/05/29	10:14:28.4	36.6	129.9	29.2	5.1	5.2	5.2	5.46	4.87
2004/06/01	11:22:17.7	37.2	130.1	10.2	3.7	3.5	–	3.85	3.56
2004/08/05	20:32:53.3	35.9	127.3	0.3	3.6	3.3	–	3.60	3.62
2005/02/20	13:18:38.8	35.4	126.2	14.1	3.5	3.4	–	3.60	3.72
2005/03/17	14:39:54.8	32.6	126.0	0.0	3.0	3.1	–	3.55	3.97
2005/03/22	06:55:33.1	33.7	130.2	6.0	–	5.1	4.7	4.83	4.60
2005/03/24	14:38:42.7	33.7	130.2	13.5	–	4.1	3.2	3.97	4.17
2005/03/25	12:03:19.9	33.8	130.1	12.9	3.9	4.3	3.6	4.27	4.08
2005/04/19	21:11:27.0	33.6	130.3	18.8	4.7	5.7	5.1	5.36	5.22
2005/04/20	00:09:43.2	33.7	130.3	20.4	4.6	5.1	4.5	5.20	4.65
2005/04/21	03:37:32.9	34.9	125.4	13.8	3.1	3.0	–	3.29	3.64
2005/06/14	22:07:04.2	33.3	126.0	10.0	3.8	3.7	-	4.26	3.92
2005/06/14	22:37:50.8	33.3	126.1	0.0	2.9	3.0	–	3.22	3.59
2005/06/20	06:31:50.6	38.7	125.8	0.0	2.7	3.0	–	3.20	3.38
2005/06/29	14:18:03.8	34.4	129.2	5.5	3.7	4.0	4.2	4.14	4.13
2005/06/29	15:25:02.5	36.7	129.8	6.4	3.1	3.1	–	3.45	3.61
2005/07/29	18:01:37.4	34.2	127.5	8.0	3.0	3.1	–	3.20	3.52
2005/08/23	20:06:24.5	34.2	127.0	7.7	3.3	3.5	–	3.73	3.83
2005/10/09	23:51:08.3	37.8	125.0	4.5	3.6	3.4	–	3.93	3.82
2005/10/21	03:00:31.5	37.8	125.0	3.3	3.2	3.0	–	3.41	3.59
2005/11/15	00:10:50.6	37.2	128.8	1.8	3.3	3.0	–	3.52	3.71
2005/11/27	02:47:09.0	38.2	124.3	19.1	2.8	3.1	–	3.44	3.69
2006/01/19	03:35:35.5	37.2	128.8	3.1	3.5	3.2	–	3.90	3.87
2006/02/13	18:31:48.6	38.9	126.0	10.0	3.2	3.0	–	3.34	3.71
2006/04/03	09:14:05.8	38.7	126.0	0.0	3.5	3.3	–	3.49	3.73
2006/04/19	00:49:34.3	37.1	129.9	7.6	2.8	3.0	–	3.35	3.57
2006/04/28	14:47:55.3	37.1	129.9	12.3	2.9	3.0	–	3.35	3.51
2006/04/29	02:01:13.1	37.1	129.9	7.8	3.2	3.5	–	3.82	3.59

Table 1

continued

Date (yyyy/mm/dd)	Time (hh:mm:ss)	Lat (°N)	lon (°E)	Dep (km)	M_L (KIGAM)	M_L (KMA)	m_b (ISC)	$m_b(Lg)$	$m_b(Pn)$
2006/05/13	10:14:31.5	34.1	129.2	24.9	3.5	–	4.3	4.06	3.89
2006/09/29	14:07:55.5	34.2	125.0	18.9	3.2	3.4	–	3.52	3.69
2007/01/20	11:56:53.6	37.7	128.6	13.1	4.9	4.8	4.4	5.24	5.07
2007/09/16	16:16:33.8	36.5	129.6	2.1	3.2	3.0	–	3.49	3.79
2007/12/31	21:33:31.1	40.4	127.1	12.5	3.3	3.0	–	4.30	3.96
2008/01/16	10:58:01.6	35.6	125.3	12.7	3.9	3.9	3.5	4.30	4.27
2008/02/29	06:53:01.0	38.8	126.2	10.0	2.7	3.2	–	3.63	3.96
2008/05/31	12:59:32.6	33.5	125.7	19.8	4.3	4.2	3.6	4.70	4.14
2008/07/23	10:29:57.8	34.5	128.1	14.5	3.2	3.2	–	3.19	3.35
2008/09/03	15:44:29.3	35.1	125.0	8.5	2.9	3.0	–	2.98	3.42
2008/10/29	00:26:15.5	36.3	127.3	5.7	3.6	3.4	–	4.10	4.06
2008/11/11	12:20:54.7	38.5	125.7	13.5	3.4	3.0	–	3.46	3.61
2008/11/11	12:30:03.7	38.5	125.7	11.2	3.3	3.0	–	3.42	3.62
2008/12/19	08:53:41.9	36.5	129.6	8.4	3.7	3.5	–	3.91	3.82
2009/02/15	13:41:58.0	35.7	125.8	18.2	3.2	3.0	–	2.81	3.33
2009/03/02	05:20:27.2	37.0	124.7	4.5	3.7	3.4	–	3.83	3.83
2009/04/02	11:27:59.1	37.6	125.9	14.6	3.2	3.0	–	3.22	3.39
2009/04/29	03:15:42.6	33.4	127.4	7.5	2.7	3.2	–	2.90	3.26
2009/05/01	22:58:28.0	36.6	128.7	11.4	3.9	4.0	3.6	4.34	4.20
2009/06/28	13:07:47.6	35.8	128.3	15.3	3.1	3.0	–	3.10	3.12
2009/07/14	19:04:49.5	35.1	125.0	6.4	3.5	3.1	–	3.66	3.87
2009/08/21	14:02:21.6	38.9	125.8	12.2	3.6	3.8	–	3.64	3.50
2010/02/09	09:08:13.7	37.4	126.8	9.5	3.3	3.0	–	3.39	3.64
2010/02/16	09:53:31.8	35.6	130.0	18.7	3.6	3.2	–	3.72	3.64
2010/02/22	14:29:30.4	33.3	127.2	4.1	3.0	3.0	–	3.06	3.55
2010/03/09	03:50:14.1	36.4	125.7	18.0	3.3	3.2	–	3.27	3.58

The reported magnitudes (M_L(KIGAM), M_L(KMA), m_b(ISC), $m_b(Lg)$) are presented along with $m_b(Pn)$ estimates

travel time curves (Hong *et al.*, 2008; Hong and Kang, 2009; Hong and Rhie, 2009), the time windows are set to be from $d/7.95 + 1$ to $d/6.8 + 4$ s, where d is the epicentral distance in km. Note that the time windows begin before the *Pn* arrivals, and ends before the *Pg* arrivals (Fig. 3). Every *Pn* record section is examined manually so as to include only the *Pn* and *Pn* coda securely. When the selected wavetrains contain *Pg* phases, the record sections are removed in the analysis. Figure 2 presents an example of regional waveform and its peak-to-peak *Pn* amplitude.

To determine the constants a and b, we rewrite Eq. (1) to be

$$\log A - M_{ref} = -a - b \log d, \qquad (2)$$

where M_{ref} is the reference magnitude for which $m_b(Lg)$ values are applied in this study. The $m_b(Lg)$ values are only available body-wave magnitude estimates for the events around the Korean Peninsula. Note that body-wave magnitude estimates based on teleseismic phases are generally unavailable since the event sizes are small. The determination of constants a and b is a calibration process. The constants a and b are determined so that the $m_b(Pn)$ estimates are comparable to the reference magnitudes.

The constants are determined using a linear regression of calibrated logarithmic *Pn* amplitudes as a function of logarithmic distances. To test the stability and reliability of the determined constants a and b, we measure the standard deviations of the data set with respect to the fitted line (Press *et al.*, 1992).

4.2. Inter-Station Magnitude Residuals

The magnitude estimates may vary by station due to influence of source radiation pattern, raypath properties, and receiver-site effect. Magnitude

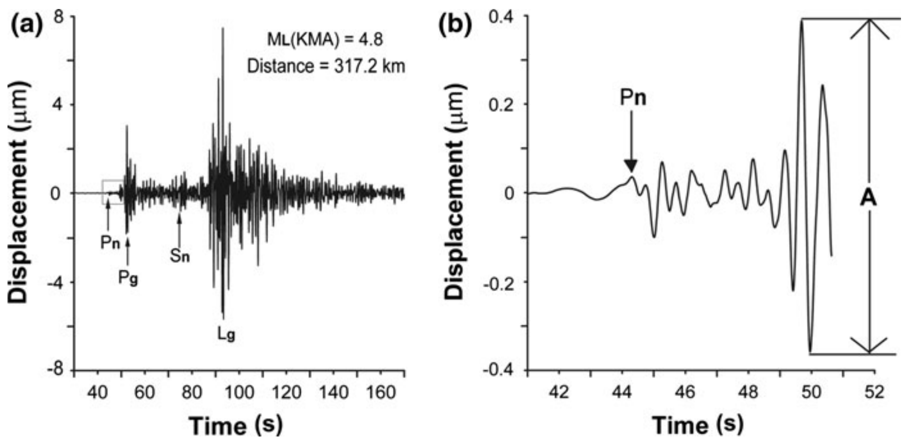

Figure 2

a A vertical regional seismogram for an M_L 4.8 earthquake at a distance of 317.2 km. Major regional phases (*Pn, Pg, Sn, Lg*) are indicated. **b** An enlarged *Pn* and *Pn* coda section that is marked with an *open rectangle* in (**a**). The peak-to-peak amplitude (*A*) is presented

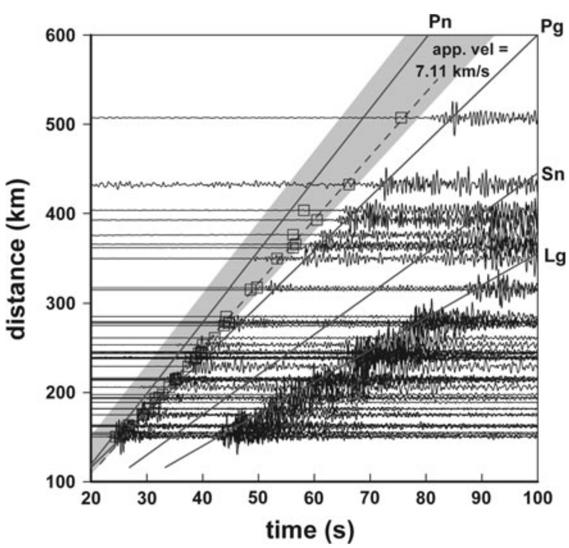

Figure 3

An example of picked wavelets for estimation of $m_b(Pn)$, and examination of consistency of picked phase. Vertical waveforms for the 20 January 2007 M_L4.8 earthquake are analyzed. The arrival times of major regional phases (*Pn, Pg, Sn, Lg*) are indicated with *solid lines*. The wavetrains analyzed for estimation of $m_b(Pn)$ are marked with a *shaded zone*. The picked wavelets with the largest peak-to-peak amplitudes are marked with *open squares*. The travel times of picked wavelets are fitted with a *dotted line* using a linear regression. Most picked wavelets are found to be clustered around the *fitted line* of which apparent velocity is determined to be 7.11 km/s

residuals with respect to the average value of individual magnitude estimates at stations reflect the relative energy variations. The assessment of receiver-site effect from seismic amplitudes requires corrections for source strengths and attenuations along raypaths, asking knowledge on source and raypath properties. In this study, we instead present a method to assess the receiver-site effect from normalized magnitude residuals.

A normalized inter-station magnitude residual can be calculated by

$$R_{ij} = \frac{m_b^{i,j} - m_b^{i,rep}}{m_b^{i,rep}}, \tag{3}$$

where $m_b^{i,j}$ is the magnitude estimate in station j for event i, and $m_b^{i,rep}$ is the representative magnitude of event i that corresponds to the average value of magnitude estimates at all stations. The $m_b(Pn)$ values in Table 1 are used for $m_b^{i,rep}$.

The stacking of magnitude residuals for evenly-distributed events minimizes the effects of source radiation patterns and raypath properties, but extracts the receiver-site effect. The average magnitude residual at station j can be calculated by stacking the normalized inter-station magnitude residuals of all events:

$$S_j = \frac{1}{n_j}\sum_{i=1}^{n_j} R_{ij}, \tag{4}$$

where n_j is the number of events observed at station j. The average magnitude residual S_j reflects the receiver-site effect on *Pn* amplification.

The seismic stations are deployed densely over the Korean Peninsula (Fig. 1), which allow us to assess the regional variation of magnitude residuals.

The regional magnitude residuals $(\Delta M/M|_{avg})$ can be calculated by stacking the magnitude residuals (S_j) of stations that are placed in the given region:

$$\left.\frac{\Delta M}{M}\right|_{avg} = \frac{1}{N}\sum_{j=1}^{N} S_j, \tag{5}$$

where N is the number of stations in the region. Note that the near-uniform distribution of events around the Korean Peninsula and stacking process enables us to calculate regional magnitude residuals with minimal influences of source and raypath effects.

5. $m_b(Pn)$ Scale and Comparisons

We test the stability of methodology by examining the consistency in picked wavelets from the designated time windows of the Pn and Pn coda. Note that the magnitude calibration procedure in the $m_b(Pn)$ scale allows us to analyze any phases as long as they are picked consistently over all record sections.

In Fig. 3, we present an example of regional record sections for the 20 January 2007 M_L 4.8 earthquake, and also mark picked wavelets. The wavelets with the largest peak-to-peak amplitudes are observed to be clustered around the fitted line with an apparent velocity of 7.11 km/s in the wavetrains. The observation suggests that common wavelets are picked in most seismograms. The apparent velocity indicates that the wavelets may be developed from scattering on lower-crust or mantle-lid heterogeneities (e.g., Kværna and Doornbos, 1991; Wagner, 1996). It is known that the scattered waves are less affected by the source radiation patterns than the primary waves, allowing stable measurement of amplitudes (e.g., Aki and Chouet, 1975; Eken *et al.*, 2004).

We determine the Pn body-wave magnitude scale, $m_b(Pn)$, from a diagram of 3,575 calibrated logarithmic amplitudes as a function of logarithmic distances (Fig. 4). The constants a and b in Eq. (2) are determined using a linear regression. The $m_b(Lg)$ values are used for M_{ref}. The $m_b(Pn)$ scale is determined to be

$$m_b(Pn) = 0.380(\pm 0.299) + \log A + 2.012(\pm 0.122)\log d, \tag{6}$$

where A is the Pn amplitude in μm, and d is the epicentral distance in km. The estimated $m_b(Pn)$ values are presented in Fig. 5 and Table 1.

We compare the $m_b(Pn)$ estimates with reported M_L, and calculate the magnitude differences (Fig. 6a). Note that body-wave magnitudes and local magnitudes are typically determined to be comparable for events with magnitudes <5 (Utsu, 1997). We, however, find that the $m_b(Pn)$ estimates for regional

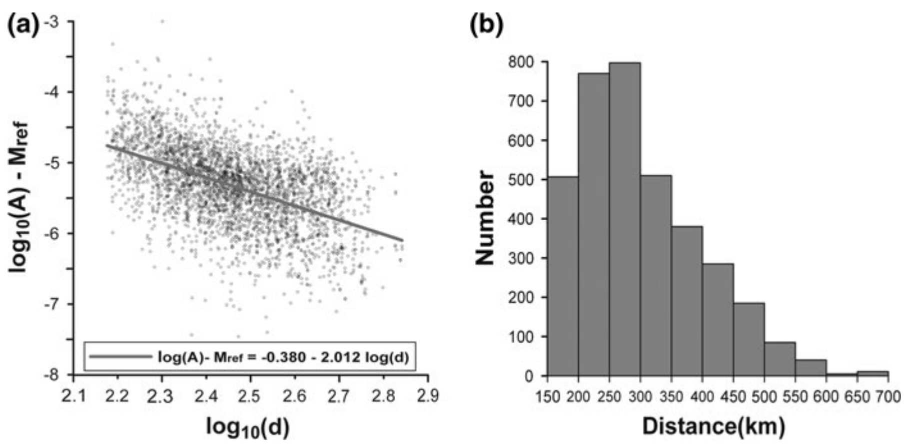

Figure 4

a Determination of constants a and b from a diagram of calibrated logarithmic amplitudes as a function of logarithmic distances. **b** Number of analyzed data as a function of epicentral distance. Waveform records with epicentral distances of 150–700 km are analyzed. The constants a and b are determined to be 0.380 and 2.012 with standard deviations of 0.299 and 0.122

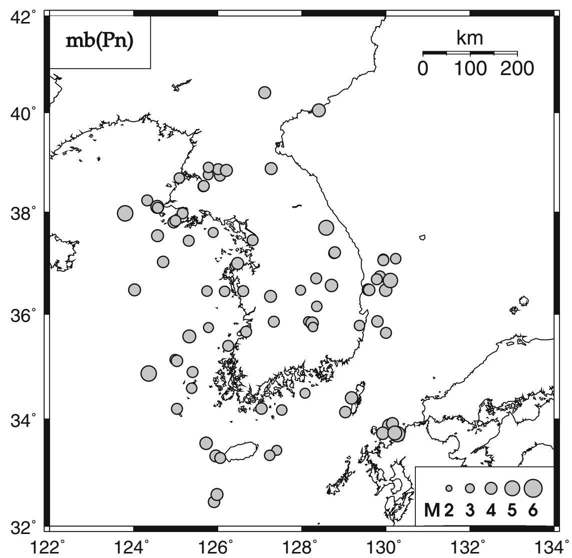

Figure 5

$m_b(Pn)$ estimates of regional events around the Korean Peninsula

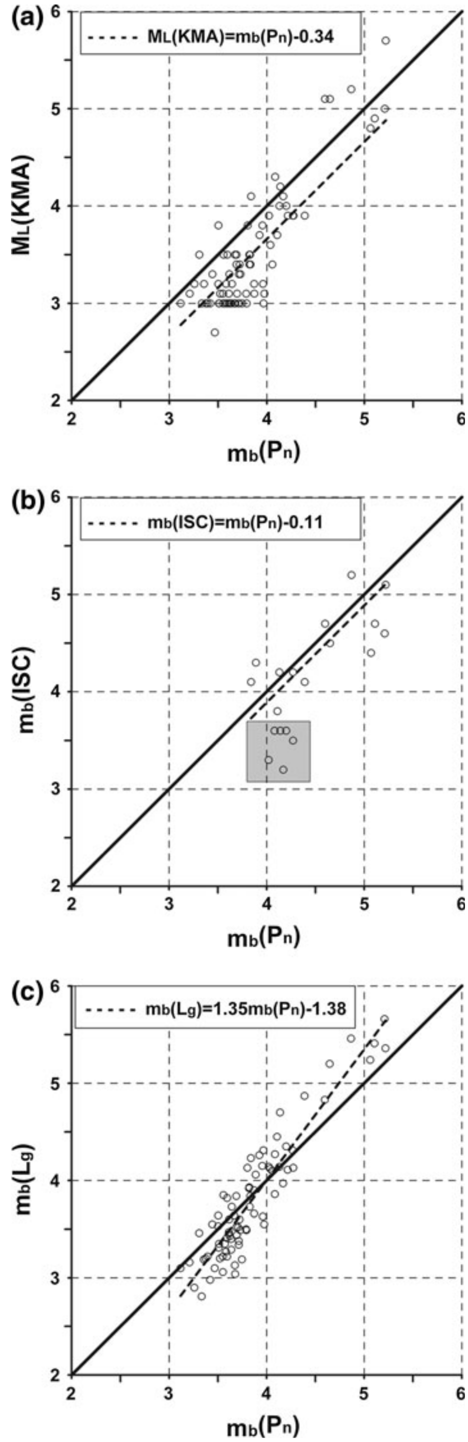

events around the Korean Peninsula are determined to be larger than M_L(KMA) by 0.34 magnitude units (mu) on average. A similar magnitude difference (0.32 mu) is observed for M_L(KIGAM). This observation is consistent with KIM and PARK (2005) that reports underestimation of magnitudes in the local magnitude scales of local institutions (KMA, KIGAM).

We compare the $m_b(Pn)$ estimates with the m_b values of the International Seismological Centre (ISC) (Fig. 6b). The m_b values of 19 events are available from the ISC (Table 1). We find that the m_b(ISC) values are larger than $m_b(Pn)$ estimates by 0.31 mu on average. We, however, find a magnitude-dependent feature between the reported m_b(ISC) and calculated $m_b(Pn)$. The m_b(ISC) is found to be lower than $m_b(Pn)$ for events with magnitudes around or less than 4 (events in the shaded box in Fig. 6b. On the other hand, $m_b(Pn)$ and m_b(ISC) are found to be nearly comparable (0.11 mu difference on average) for events with magnitudes >4.

The event-size dependent feature between m_b(ISC) and $m_b(Pn)$ may be associated with the observational distance limit depending on the event size; small events are observed only up to near-regional distances where seismic waves are strongly influenced by crustal structures. The complex crustal structures around the Korean Peninsula may cause apparent attenuation of local and regional seismic waves, yielding underestimation of magnitudes (HONG, 2012).

Figure 6

◀ Comparisons between $m_b(Pn)$ estimates and other magnitude values: **a** M_L(KMA), **b** m_b(ISC) and **c** $m_b(Lg)$. The m_b(ISC) values of 19 events are available. The $m_b(Pn)$ estimates are determined to be larger than M_L(KMA) by 0.34 mu. The $m_b(Pn)$ estimates are comparable to m_b(ISC) for events with magnitudes >4. Small events (*shaded box* in the figure) are excluded in the comparison. Characteristic mild magnitude differences depending on the magnitude sizes are observed between $m_b(Pn)$ and $m_b(Lg)$. The $m_b(Pn)$ estimates are determined to be larger than $m_b(Lg)$ for events with $m_b(Pn) < 4$, and vice versa for events with $m_b(Pn) > 4$. The overall relationship between $m_b(Pn)$ and $m_b(Lg)$ is determined to be $m_b(Lg) = 1.35\ m_b(Pn) - 1.38$

We now compare the $m_b(Pn)$ estimates with $m_b(Lg)$ values (Fig. 6c). The $m_b(Lg)$ values are used as the reference body-wave magnitudes of events in this study. The $m_b(Pn)$ scale was determined so that the overall magnitude estimates are comparable to the reference magnitudes. We find that the average magnitude difference between $m_b(Pn)$ and $m_b(Lg)$ is determined to be nearly zero.

We, however, find a mild event-size-dependent feature in magnitude differences. The $m_b(Pn)$ estimates are observed to be larger than the $m_b(Lg)$ by 0.13 mu on average for events with $m_b(Pn) < 4$. On the other hand, the $m_b(Lg)$ values are larger than the $m_b(Pn)$ by 0.18 mu on average for events with $m_b(Pn) > 4$. We find the overall relationship between $m_b(Pn)$ and $m_b(Lg)$ to be (Fig. 6c)

$$m_b(Lg) = 1.35 m_b(Pn) - 1.38. \tag{7}$$

The mild magnitude differences between $m_b(Pn)$ and $m_b(Lg)$ are observed in other regions (Priestley and Patton, 1997). The magnitude differences may be caused by the discrepancy in spectral contents between mantle-lid waves and crustal-guided waves that vary also with event sizes (e.g., Hong and Rhie, 2009).

The magnitude differences between $m_b(Pn)$ and $m_b(Lg)$ are further investigated from their spatial variations (Fig. 7). It is shown that the magnitude differences are high in offshore events. The $m_b(Pn)$ estimates are determined to be larger than $m_b(Lg)$ for events off the west coast, while in inverse for those off the east coast. On the other hand, the $m_b(Pn)$ estimates are determined to be comparable to the $m_b(Lg)$ for inland events. This spatial feature suggests that the magnitude differences may be a result of discriminative seismic attenuations that vary by phase and

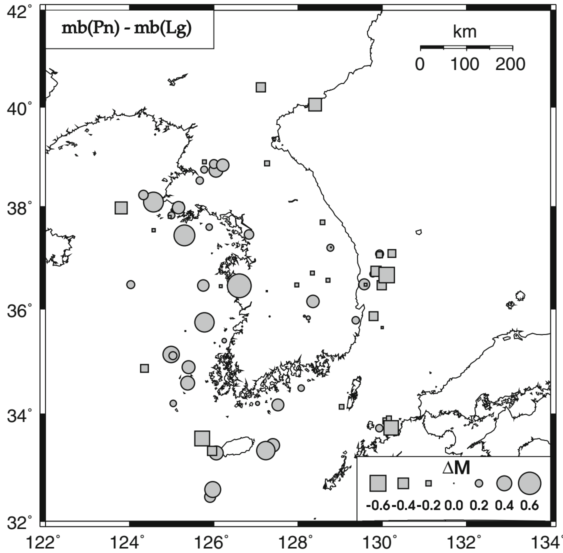

Figure 7

Spatial variation of magnitude differences between $m_b(Pn)$ and $m_b(Lg)$ estimates. The $m_b(Pn)$ estimates are larger than $m_b(Lg)$ for events around the west coast of the peninsula. The $m_b(Pn)$ estimates are lower than the $m_b(Lg)$ for events around the east coast

raypath. The discriminative attenuations are strong in record sections for events with narrow-azimuthal coverage due to dominant reflection of local raypath properties, causing discriminative phase-dependent spectral modulation. Thus, it appears that good azimuthal coverage may be desirable for stable estimation of magnitudes of regional events.

6. *Magnitude Residuals and Implications*

We investigate inter-station magnitude residuals, and infer the receiver-site-dependent Pn amplification. The inter-station magnitude residuals are calculated from Eq. (3). Figure 8 presents examples of inter-station magnitude residuals for two single events, which are the 20 June 2005 $m_b(Pn)$ 3.38 earthquake and the 20 January 2007 $m_b(Pn)$ 5.07 earthquake. We find consistent spatial variations in the magnitude residuals. Here, note that the inter-station magnitude residuals for a single event reflects not only the receiver-site effect, but also the source and raypath effects. Thus, the magnitude residuals are discordant between the events at some common stations.

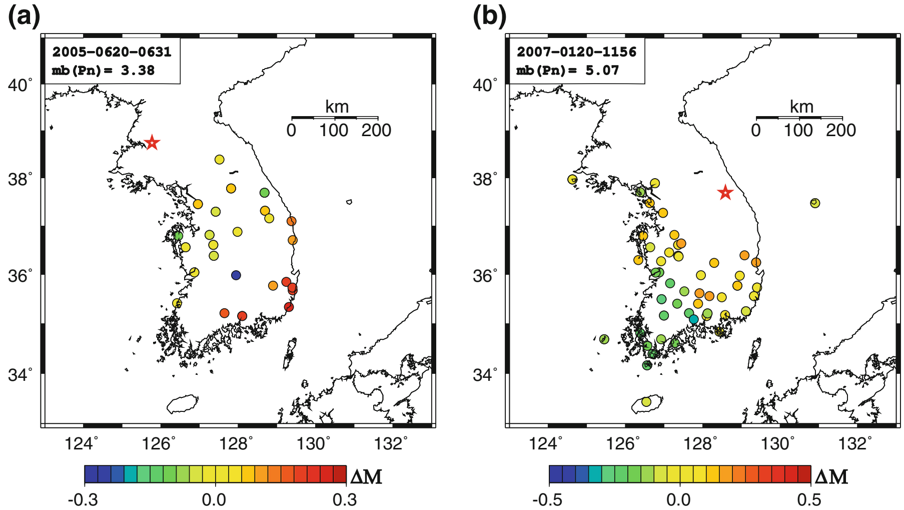

Figure 8
Magnitude residuals at stations for two selected events: **a** the 20 June 2005 $m_b(Pn)$ 3.38 earthquake and **b** the 20 January 2007 $m_b(Pn)$ 5.07 earthquake. The station locations are marked with *circles*, and the event locations with *stars*. The magnitude residuals vary up to ±10 % with respect to the reference magnitudes

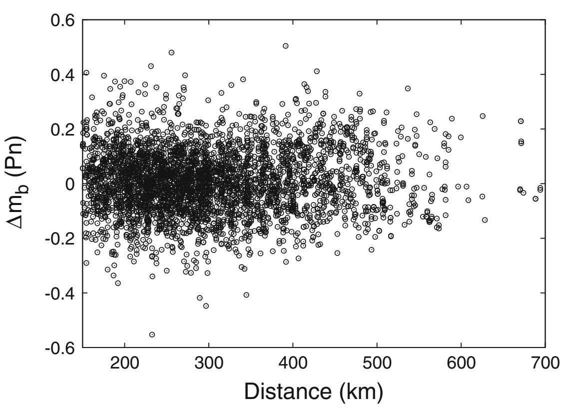

Figure 9
Magnitude residuals ($\Delta m_b(Pn)$) as a function of epicentral distance for all event records. The magnitude residuals are clustered in a range between −0.2 and 0.2 mu. The magnitude residuals are distributed evenly around zero in the entire distances

We now test the reliability of the magnitude residuals. Figure 9 presents the magnitude residuals of all events as a function of epicentral distance. Most magnitude residuals are calculated to be between −0.2 and 0.2 mu, and appear to be evenly distributed around zero. The observation suggests stable determination of $m_b(Pn)$ estimates in the entire distances of 150–700 km.

We stack the inter-station magnitude residuals for all events using Eq. (4), and calculate the average inter-station magnitude residuals (S_j) at common stations. From Eq. (5), we then calculate the representative regional magnitude residuals by averaging the magnitude residuals of stations belonging to the region. The study region is set by 33°N-39°N in latitude and 124–132°E in longitude. The region is discretized by 0.8° by 0.8° bins. Each bin overlaps with neighboring bins by 0.7° in latitude and longitude. The numbers of data are 100 or more in most bins (Fig. 10a). The western and central regions of the peninsula display large numbers of observations, while the northern regions present relatively small numbers of observations.

We present the stacked magnitude residuals for bins with numbers of data greater than or equal to 20, covering most regions of the southern Korean Peninsula. Most stacked normalized magnitude residuals vary between −0.06 and 0.06, suggesting site-dependent magnitude variations up to ±6 % (Fig. 10b). We find a large normalized magnitude residuals of ∼0.1 in the Jeju island, a Cretaceous volcanic island. Also, we find positive magnitude residuals (i.e., seismic amplification relative to the average) around a Cretaceous sedimentary basin (Gyeongsang basin) in the southeastern Korean Peninsula. On the other hand, negative magnitude residuals (i.e., seismic deamplification relative to the

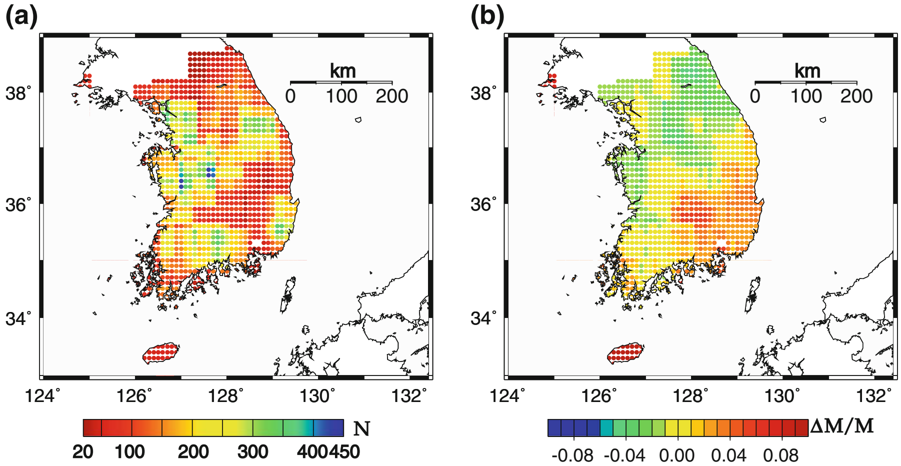

Figure 10

Spatial variation of stacked inter-station magnitude residuals: **a** numbers (*N*) of observations, and **b** stacked normalized magnitude residuals ($\Delta M/M|_{avg}$). The regional magnitude residuals are calculated for 0.8° × 0.8° bins. Results for bins with numbers of data ≥20 are presented. Large numbers of data are observed in most regions. Most stacked normalized magnitude residuals vary between −0.06 and 0.06. High positive magnitude residuals are observed in the southeastern Korean Peninsula. High negative magnitude residuals are observed in the central regions of the peninsula

average) are observed around the Gyeonggi massif region. The magnitude residuals are determined to be close to zero around the Okcheon fold belt region (see Fig. 1a).

The positive magnitude residuals indicate that the observed *Pn* amplitudes are larger than the averages, while the negative magnitude residuals suggest lower amplitudes. The spatial variation of magnitude residuals appears to be highly correlated with the geological structures that are well envisaged by seismic velocities (Kang and Shin, 2006; Hong and Kang, 2009). This observation suggests that the crustal properties beneath stations affect *Pn* amplification.

7. Discussion and Conclusions

The mantle-lid *P* wave, *Pn*, is the first-arrival phase in regional distances. The *Pn* waves are well observed in complex tectonic regions including continental margins. The *Pn* waves are useful for assessment of magnitudes of regional events including underground nuclear explosions that excite strong *P* energy (e.g., Hong *et al.*, 2008; Hong and Rhie, 2009).

In this study, we developed a *Pn* body-wave magnitude scale ($m_b(Pn)$) based on simulated SP WWSSN waveforms. We measured the $m_b(Pn)$ values of regional events around the Korean Peninsula during 2000–2010. The $m_b(Pn)$ estimates are determined to be larger than the M_L values of local institutes by 0.32–0.34 magnitude units on average. The observation suggests that the local magnitudes can be underestimated in regions with abrupt changes of crustal structures like the Korean Peninsula. The $m_b(Pn)$ estimates are determined to be larger than the $m_b(Lg)$ for events with magnitudes lower than 4. On the other hand, the $m_b(Pn)$ is determined to be lower than $m_b(Lg)$ for events with magnitude larger than 4.

We also find a characteristic spatial variation of magnitude differences between $m_b(Pn)$ and $m_b(Lg)$; the $m_b(Pn)$ estimates are determined to be larger than the $m_b(Lg)$ for events off the west coast, while the $m_b(Lg)$ estimates are larger than the $m_b(Pn)$ for those off the east coast. On the other hand, the $m_b(Pn)$ estimates are determined to be similar to the $m_b(Lg)$ for inland events. This feature may be developed by discriminative attenuation of *Pn* and *Lg* along raypaths in offshore regions, causing nonuniform variations of spectral contents of phases.

The magnitude residuals are calculated for inland regions where $m_b(Pn)$ and $m_b(Lg)$ are determined to be similar. The stacking of magnitude residuals for scattered events and stations allows us to minimize the source and raypath effects. The stacked normalized magnitude residuals vary between −0.1 and 0.1, suggesting up to 10 % variation of magnitudes. The Cretaceous sedimentary region in the southeast Korean Peninsula presents high positive magnitude residuals, while the massif regions in the central peninsula display high negative magnitude residuals. We observe that the magnitude residuals are highly correlated with the geological and seismic structures. The magnitude residuals suggest that the *Pn* amplitudes are influenced by the crustal structures beneath the stations.

Acknowledgments

We are grateful to the Korea Meteorological Administration (KMA) and the Korea Institute of Geoscience and Mineral Resources (KIGAM) for making seismic data available. We thank the editor-in-chief, Professor Brian Mitchell, and two anonymous reviewers for constructive and careful review comments that improved the manuscript. This work was supported by the Korea Meteorological Administration Research and Development Program under Grant CATER 2012-8050.

References

Aki, K., and Chouet, B., (1975), *Origin of coda waves: Source, attenuation and scattering effects*, J. Geophys. Res., *80*, 3322–3342.

Chang, S.-J., and Baag, C.-E., (2005), *Crustal structure in southern Korea from joint analysis of teleseismic receiver functions and surface-wave dispersion*, Bull. Seism. Soc. Am., *95* (4), 1516–1534.

Cho, H.-M., Kim, H.-J., Jou, H.-T., Hong, J.-K., and Baag, C.-E., (2004), *Transition from rifted continental to oceanic crust at the southeastern Korean margin in the East Sea (Japan Sea)*, Geophys. Res. Lett., *31*, L07606, doi:10.1029/2003GL019107.

Choi, H., Hong, T.-K., He, X., and Baag, C.-E., (2012), *Seismic evidence for reverse activation of a paleo-rifting system in the East Sea (Sea of Japan)*, Tectonophysics, (in press).

Chough, S.K., Kwon, S.-T., Ree, J.-H., and Choi, D.K., (2000), *Tectonic and sedimentary evolution of the Korean peninsula: a review and new view*, Earth-Science Reviews, *52*, 175–235.

Denny, M.D., Taylor, S.R., and Vergino, E.S., (1987), *Investigation of m_b and M_S formulas for the western United States and their impact on the M_S/m_b discriminant*, Bull. Seism. Soc. Am., *77*, 987–995.

Eken, T., Mayeda, K., Hofstetter, A., Gök, R., Örgülü, G., and Turkelli, N., (2004), *An application of the coda methodology for moment-rate spectra using broadband stations in Turkey*, Geophys. Res. Lett., *31*, L11609, doi:10.1029/2004GL019627.

He, X., and Hong, T.-K., (2010), *Evidence for strong ground motion by waves refracted from the Conrad discontinuity*, Bull. Seism. Soc. Am., *100* (3), 1370–1374.

Helmberger, D., Dreger, D., Stead, R., and Kanamori, H., (1993), *Impact of broadband seismology on the understanding of strong motions*, Bull. Seism. Soc. Am., *83* (3), 830–850.

Hong, T.-K., (2010), *Lg attenuation in a region with both continental and oceanic environments*, Bull. Seism. Soc. Am., *100* (2), 851–858.

Hong, T.-K., (2012), *Lg body-wave magnitude scaling for the continental margin around Korea and Japan*, Pure Appl. Geophys., (in press).

Hong, T.-K., Baag, C.-E., Choi, H., and Sheen, D.-H., (2008), *Regional seismic observations of the October 9, 2006 underground nuclear explosion in North Korea and the influence of crustal structure on regional phases*, J. Geophys. Res., *113*, B03305, doi:10.1029/2007JB004950.

Hong, T.-K., and Kang, T.-S., (2009), *Pn traveltime tomography of the paleo-continental-collision and rifting zone around Korea and Japan*, Bull. Seism. Soc. Am., *99* (1), 416–421.

Hong, T.-K., and Rhie, J., (2009), *Regional source scaling of the 9 October 2006 underground nuclear explosion in North Korea*, Bull. Seism. Soc. Am., *99* (4), 2523–2540.

Kang, T.-S., and Shin, J.S., (2006), *Surface-wave tomography from ambient seismic noise of accelerograph networks in southern Korea*, Geophys. Res. Lett., *33*, L17303, doi:10.1029/2006GL027044.

Kennett, B.L.N., (1986), *Lg waves and structural boundaries*, Bull. Seism. Soc. Am., *76*, 1133–1141.

Kennett, B.L.N., and Furumura, T., (2001), *Regional phases in continental and oceanic environments*, Geophys. J. Int., *146* (2), 562–568.

Kim, W.-Y., (1998), *The M_L scale in eastern North America*, Bull. Seism. Soc. Am., *88*, 935–951.

Kim, H.-J., Jou, H.-T., Cho, H.-M., Bijwaard, H., Sato, T., Hong, J.-K., Yoo, H.-S., and Baag, C.-E., (2003), *Crustal structure of the continental margin of Korea in the East Sea (Japan Sea) from deep seismic sounding data: evidence for rifting affected by the hotter than normal mantle*, Tectonophysics, *364*, 25–42.

Kim, S.K., and Park, M.A., (2005), *The local magnitude scale in the Korean Peninsula*, Pure. Appl. Geophys., *162*, 875–889.

Korea Institute of Geology and Mineral Resources (KIGAM) (1995), Seismological Study in the Kyungsang Basin (II), KIGAM Res. Rep. KR-95(C)-5, 79 pp. (in Korean).

Korea Meteorological Administration (KMA) (1999), Investigation of Body-wave Attenuation and Tsunami Simulation, Ministry of Sci. Techn. 206 pp. (in Korean).

Kværna, T., and Doornbos, D.J., (1991), *Scattering of regional Pn by Moho topography*, Geophys. Res. Lett., *18*, 1273–1276.

Leach Jr., R.R., Dowla, F.U., and Vergino, E.S., (1993), *Yield estimation using bandpass-filtered seismograms: Preli minary results using neural networks with mb(Pn), short-time, long-time, and coda energy measurements*, Bull. Seism. Soc. Am., *83*, 488–508.

Nuttli, O.W., (1986), *Yield estimates of Nevada test site explosions obtained from seismic Lg waves*, J. Geophys. Res., *91*, 2137–2151.

Patton, H.J., (2001), *Regional magnitude scaling, transportability, and Ms:mb discrimination at small magnitudes*, Pure Appl. Geophys., *158* (11), 1951–2015.

Patton, H.J., and Schlittenhardt, J., (2005), *A transportability $m_b(Lg)$ scale for central Europe and implications for low-magnitude M_s-m_b discrimination*, Geophys. J. Int., *163*, 126–140.

PRESS, W.H, TEUKOLSKY, S.A., VETTERLING, W.T., and FLANNERY, B.P., (1992), Numerical Recipes in Fortran: The Art of Scientific Computing, 2nd ed., Cambridge University Press, New York, USA, pp 963.

PRIESTLEY, K.F., and PATTON, H.J., (1997), *Calibration of* $m_b(Pn)$, $m_b(Lg)$ *scale and transportability of the* M_0:m_b *discriminant to new tectonic regions*, Bull. Seism. Soc. Am., *87* (5), 1083–1099.

UTSU, T., (1997), *Relationships between magnitude scales*, in International Handbook of Earthquake and Engineering Seismology, Part A, eds. H.K. LEE, H. KANAMORI, P.C. JENNINGS, and C. KISSLINGER, Academic Press, London, UK, p 933.

VERGINO, E.S., and MENSING, R.W., (1990), *Yield estimation using regional mb(Pn)*, Bull. Seism. Soc. Am., *80*, 656–674.

WAGNER, G.S., (1996), *Numerical simulations of wave propagation in heterogeneous wave guides with implications for regional wave propagation and the nature of lithospheric heterogeneity*, Bull. Seism. Soc. Am., *86* (4), 1200–1206.

YIN, A., and NIE, S., (1993), *An indentation model for the north and south China collision and development of the Tan-Lu and Honam fault systems, eastern Asia*, Tectonics, *12*, 810–813.

(Received August 28, 2011, revised January 24, 2012, accepted January 31, 2012, Published online April 3, 2012)